Journal of
Materials Chemistry A

Materials for energy and sustainability

Accepted Manuscript

This article can be cited before page numbers have been issued, to do this please use: D. Samanta, M. Kumar, S. Singh, P. Verma, K. K. Kar, T. K. Maji and M. K. Ghorai, *J. Mater. Chem. A*, 2020, DOI: 10.1039/D0TA02318C.

ROYAL SOCIETY OF CHEMISTRY

rsc.li/materials-a

View Article Online
DOI: 10.1039/D0TA02318C

Journal Name

COMMUNICATION

Triphenylamine and terpyridine–Zinc(II) complex based donor-acceptor soft hybrid as visible light-driven hydrogen evolution photocatalyst

Received 00th January 20xx,
Accepted 00th January 20xx

DOI: 10.1039/x0xx00000x

www.rsc.org/

Debabrata Samanta,*[a] Manish Kumar,[a] Sugandha Singh,[b] Parul Verma,[c] Kamal K. Kar,*[b] Tapas Kumar Maji*[c] and Manas K Ghorai*[a]

A donor-acceptor coordination polymer (TPA-Zn) was synthesized by Zn(II)-assisted self-assembly of an *in situ* generated triphenylamine (TPA) cored tristerpyridine ligand. The polymer absorbs broad-spectrum of light and exhibits visible light-assisted hydrogen generation (27.1 mmol g^{-1} over 9 h) from water with 2.9% quantum efficiency at 400 nm. The microscopic images represent mesoscale fibrous morphology and Brunauer-Emmett-Teller (BET) analysis reveals porous nature of TPA-Zn (surface area: 234.5 m^2/g; *d* = 6.98 nm), both are helping to substrate diffusion during catalysis.

The ever-increasing energy demand of our society and concomitant rapid decline of non-renewable energy sources urgently require development of alternative energy sources.[1] To overcome the energy crisis, researchers have been designing and synthesizing new materials to harvest sunlight as an alternative source of energy, but the challenge remains in systematic conversion into clean energy materials.[2] The visible light-induced photocatalytic H_2 generation through water oxidation has received enormous interest as H_2 serves as a source of high energy density and clean energy material.[3] Several metal-organic hybrid systems as well as π-conjugated organic polymers such as hydrazine and triazine-cored covalent organic frameworks, graphitic C_3N_4 and other nitrogen containing conjugated organic polymers have been developed for this purpose.[4-6] The basic designing principle of such catalyst relies on broad area of visible light absorption with substantial photoexcited lifetime. Additionally, an efficient photocatalyst requires high charge carrier (CC) mobility and exciton separation (ES) ability.[7] The high CC mobility is achieved by extended π-conjugation. Unfortunately, the extended conjugation decreases ES ability and reduces photocatalytic performance.[8] To enhance ES, donor-acceptor (D-A) π-conjugated organic polymers have recently been developed, but the D-A functionality generates polarization on the π-conjugated backbone which reduces the CC mobility.[8,9] Therefore, an optimum value of ES ability and CC mobility is desirable in an efficient photocatalyst. A metal-organic hybrid system with proper selection of metal ion and moderately high π-conjugated organic ligand could provide the optimum values of ES and CC mobility, and thus display high catalytic efficiency. The metal ion should disrupt inter-ligand π-electronic communication. The hybrid materials can also be porous which further facilitates the essential substrate-catalyst interaction.[10] Moreover, downsizing the material into meso/nanoscale dimension would allow easy solution dispersibility and lessen the diffusion barrier of substrate into catalytic centers.[10]

Triphenylamine derivatives (TPA) have significantly high lifetime of charge separated state.[11] Additionally, by virtue of electron richness, the *N*-centre of TPA could also act as weak proton binder during photocatalytic hydrogen production. Therefore, we envisaged that TPA and alkoxy chains embedded moderately high π-conjugated organic-inorganic hybrid materials could be a promising photocatalyst for hydrogen production (scheme 1). The alkoxy sidechains could generate meso/nanoscale coordination polymer resulting in enhanced substrate diffusion.[12] In the present work, we have therefore designed and synthesized a novel coordination polymer **TPA-Zn** utilizing zinc (II) ion and an *in situ* synthesized TPA-cored moderately high π-conjugated tristerpyridine ligand (Figure 1). The zinc (II) (d^{10} system) ions provide intermittent disruption in CC mobility. The microscopic studies revealed inter-connected fibrous morphology generating mesopores (*d* = 7-15 nm) as analysed by N_2 adsorption at 77 K. The material displayed visible light absorption

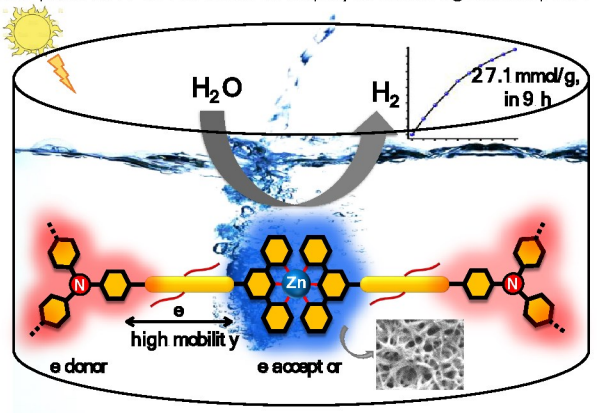

Scheme 1: Schematic representation of the present work showing visible light-induced dihydrogen production by the mesoscale coordination polymer **TPA-Zn**.

[a]*Department of Chemistry, Indian Institute of Technology, Kanpur 208016, India E-mail: dsamanta@iitk.ac.in (DS); E-mail: mkghorai@iitk.ac.in (MKG)*
[b]*Advanced Nanoengineering Materials Laboratory, Materials Science Programme and Department of Mechanical Engineering, Indian Institute of Technology Kanpur, Kanpur-208016, India. E-mail: kamalkk@iitk.ac.in*
[c]*Molecular Materials Laboratory, Chemistry and Physics of Materials Unit, Jawaharlal Nehru Centre for Advanced Scientific Research, Bangalore-560064, India E-mail: tmaji@jncasr.ac.in*
Electronic Supplementary Information (ESI) available: DOI: 10.1039/x0xx00000x

View Article Online
DOI: 10.1039/D0TA02318C

Figure 1: (a) Synthesis scheme and (b) chemdraw structure of the coordination polymer **TPA-Zn** along with digital photograph as inset. (c) N_2 adsorption isotherm at 77 K and (b) XPS analysis (showing Zn region only) of **TPA-Zn**.

and EPR spectroscopy indicated substantial charge-separation in the ground state. The **TPA-Zn** was found to produce 30.1 mmol g^{-1} and 55.6 mmol/g of dihydrogen in 16 hours from water/triethylamine (v/v = 19:1) medium under visible light (420-750 nm) and broad-spectrum irradiation (290-750 nm), respectively. The quantum efficiency of the photocatalysis was calculated to be 2.9% at 400 nm. The catalyst is highly recyclable and does not require any co-catalyst. The required ligand **5** for the synthesis of **TPA-Zn** was prepared via Pd(0) catalysed Sonogashira cross-coupling reactions (Figure 1a). At first, 1,4-dibutoxy-2,5-diiodobenzene (**1**) was selectively mono-coupled with 4-ethynylbenzaldehyde (**2**) to afford **3** with 54% yield and then **3** was further coupled with ethynylterpyridine (**4**) to furnish the terpyridylaldehyde ligand **5** with 86% yield. The targeted coordination polymer **TPA-Zn** was finally synthesized by the self-assembly between Zn(II) ions and an *in situ* generated TPA-cored tris-terpyridine ligand **TPA-tpy** (Figure S1), produced via Schiff base condensation between tris(4-aminophenyl)amine and **5** (Figure 1b). The **TPA-Zn** was produced as a black solid with 91% yield and characterized by physicochemical methods. The molecular formula of **TPA-Zn** was determined by inductively coupled plasma mass spectrometry (ICP-MS), energy-dispersive X-ray spectroscopy (EDAX), thermogravimetric analysis (TGA) and elemental analysis. The ICP-MS and EDAX analyses of **TPA-Zn** indicated the presence of 3.71 and 4.07 wt % Zn, respectively (Figure S2). The material does not contain any solvent/water in the framework as the TGA showed no significant weight loss up to 232 °C (Figure S3). Finally, the elemental analysis proposed chemical formula of **TPA-Zn** as $[Zn_{1.5}$(**TPA-tpy**)$](OTf)_3$. Fourier-transform infrared (FT-IR) spectroscopy indicated the absence of aromatic amine (3250-3500 cm^{-1}) functionality, suggesting that the amine group was converted to imine and the corresponding stretching frequency appeared at 1689 cm^{-1} (Figure S4). The x-ray photoelectron spectroscopy (XPS) of **TPA-Zn** confirms the presence of Zn(II) along with C, N, O, S and F atoms (Figure 1d/S5). The binding energies of Zn 2p core level electrons were observed at 1019.5 eV ($2p_{3/2}$) and 1042.4 eV ($2p_{1/2}$). The TPA-Zn was further characterized by ^{13}C NMR spectroscopy in solid state. The spectrum displayed characteristic broad ^{13}C NMR signals for alkyl, alkyne, imine and zinc-complexed terpyridyl α-carbons at 29.8-49.5, 90.4, 151.8 and 179.1 ppm, respectively (Figure S6). The powder X-ray diffraction (PXRD) analysis of **TPA-Zn** revealed amorphous nature of the polymer (Figure S7). The degassed **TPA- Zn** showed type-II N_2 adsorption isotherm at 77 K with a final uptake of 406 $cm^3\ g^{-1}$ at p = 1 atm, highlighting permanently porous nature of the polymer (Figure 1c/S8). BET analysis of the isotherm revealed surface area of **TPA-Zn** as 234.5 $m^2\ g^{-1}$. The nonlocal density functional theoretical fitting indicated a distribution of mesopores ranging from 6.99 to 15.2 nm, possibly arises due to random stacking of inter-connected fibrous network (fibre width: ~200-900 nm) as clearly observed in transmission electron microscopy (TEM) and field emission scanning electron microscopy (FESEM) (Figure 2d,e/S9/S10). The elemental colour mapping showed uniform distribution of C, N, O, S, F and Zn in **TPA-Zn** (Figure 2f).

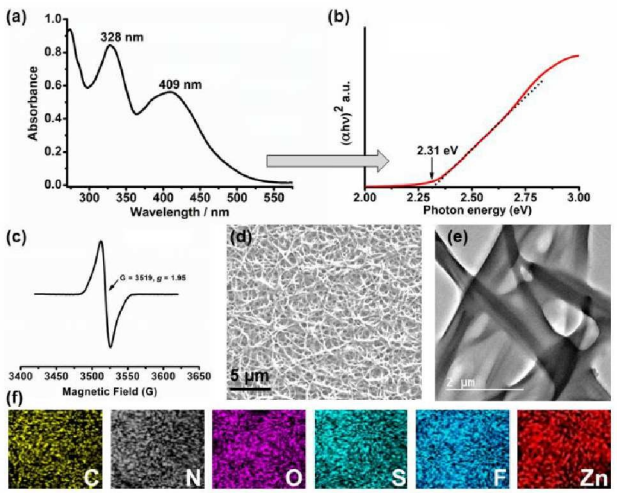

Figure 2: (a) UV-Vis absorption spectrum and (b) Tauc plot of **TPA-Zn** in aqueous dispersion. (c) EPR spectrum of **TPA-Zn** in solid state at room temperature. (d) FESEM and (e) TEM images, and (f) Elemental colour mapping of **TPA-Zn**.

View Article Online
DOI: 10.1039/D0TA02318C

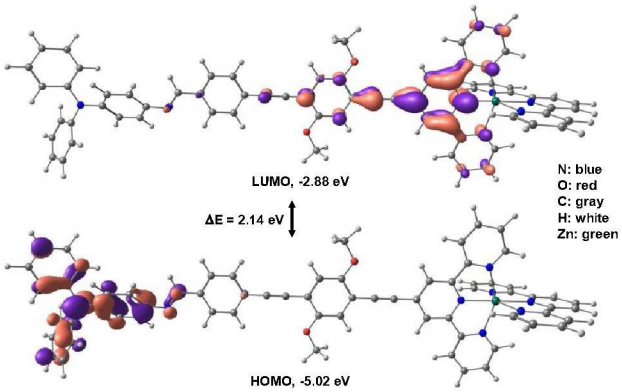

Figure 3: D3-B3LYP/6-31G(d) calculated HOMO-LUMO diagrams (contour value = 0.04) of a **TPA-Zn** model system in water.

With a perspective of photocatalysis, the band gap (Eg) of **TPA-Zn** was derived from UV-Vis spectroscopy using Tauc Plots. The UV-Vis absorption spectroscopy of **TPA-Zn**, measured as aqueous dispersion, revealed broad area of visible light absorption upto 552 nm with λ_{max} = 409 nm (Figure 2a, S11). The **TPA-Zn** showed yellow emission with a maximum at 561 nm (λ_{exc} = 409 nm). The absolute quantum yield and excited state lifetime were measured to be 7.9% and 1.80 ns, respectively (Figure S12). Transformation of the UV-Vis spectrum into $(\alpha h\upsilon)^2$ vs. photon energy plot unveiled the band gap as 2.31 eV, indicating facile charge mobility in **TPA-Zn** (Figure 2b). A density functional theoretical (DFT) calculation, at D3-B3LYP/6-31G(d) level, presented the highest occupied molecular orbital (HOMO) on the electron-rich TPA unit and the lowest unoccupied molecular orbital (LUMO) on the Zn(II)-coordinated electron-deficient terpyridyl units with the HOMO-LUMO gap of 2.14 eV, which is in good agreement with the experimentally evaluated band gap (Figure 3). The electron paramagnetic resonance (EPR) revealed a sharp and intense signal at g = 1.95, indicating that **TPA-Zn** exist as a charge-separated species (Figure 2c). Both the DFT and EPR studies indicated that TPA acts as a donor whereas terpyridyl units act as acceptor in **TPA-Zn**. The observations are indicative for facile exciton separation which is necessary for the photocatalysis. Moreover, the model system of **TPA-Zn** was also optimized as a charge-separated species by restricting a positive charge on TPA and a negative charge on the Zn-terpyridine complex. The optimized charge-separated state was found to be higher in energy by 5.3 kcal/mol from its ground state. This indicates 5.87% existence of charge-separated state at room temperature in **TPA-Zn** (see ESI).

The heterogenous photocatalytic activity of **TPA-Zn** towards H_2 production from water was achieved in the presence of triethylamine which acts as hole scavenger during photocatalysis. The light irradiation onto the sample was performed utilizing a xenon lamp (290 W) which produces full range light of 290 - 750 nm. During visible light assisted photocatalysis, a simulated visible light of 420-750 nm was generated through a filter. In a general procedure of photocatalysis, 1.5 mg of **TPA-Zn** was dispersed into water (38 mL) and triethylamine (2 mL), and the solution was degassed by purging argon for 10 min. The solution was then irradiated either with full range or visible light, and the produced dihydrogen was quantified every hour by gas chromatography (Agilent Technologies, 7890B). Upon full range light irradiation (290 - 750 nm), **TPA-Zn** exhibited hydrogen evolution with a final amount of 55.6 mmol g^{-1} in 16 h and then saturation occurred (Figure 4a). The average rate of hydrogen production was calculated to be 5.34 mmol g^{-1} h^{-1} in 9 h and then it was slowed down to 1.07 mmol g^{-1} h^{-1} in the next 7 h (Figure 4c). The recyclability of the photocatalyst was tested upto seven cycles with intermittent degassing the dispersion in every 6 h. After each degassing step, GC-MS analysis was performed to confirm complete removal of hydrogen. No significant change in the hydrogen production was observed in the recyclability test, indicating that dispersed **TPA-Zn** is stable under full range light irradiation (Figure 4b). As the catalyst **TPA-Zn** showed significant amount of visible light absorption, we opted for photocatalytic hydrogen evolution under simulated visible light (420 – 750 nm). Similar to full rage light, the photocatalytic hydrogen evolution under visible light reached saturation in 16 h with the final amount of 30.1 mmol g^{-1} hydrogen evolution (Figure 4a). The relatively lower amount of hydrogen production under visible light may be attributed to lower amount of photon absorption by the catalyst. The average rate of hydrogen production was found to be 3.01 mmol g^{-1} h^{-1} over 9 h. Quantum efficiency of the photocatalysis was determined by using a 400 nm filter having 0.8 mW cm^{-2} s^{-1} power density (see ESI). A total of 1.77 µmol dihydrogen was produced after 1 h of light irradiation through a tubular shaped sample cell (d = 4 cm). The calculated quantum efficiency of the photocatalysis is 2.9% which is comparable with several benchmark photocatalysts (Table S1).[4] Similar to that of full range photo-irradiation, the recyclability test upto seven cycles under visible light showed no significant change in hydrogen evolution (Figure 4b). The UV-Vis absorption spectrum of **TPA-Zn**

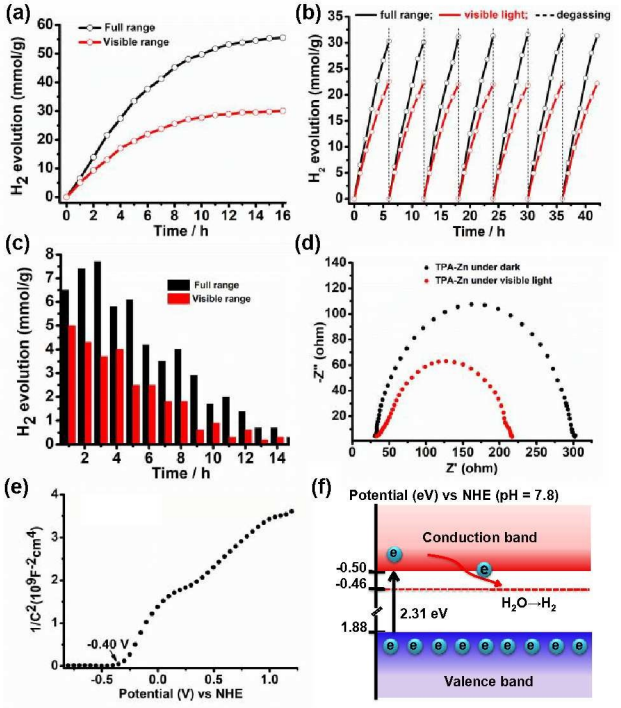

Figure 4: (a) Photocatalytic hydrogen evolution along with (b) recyclability test of the catalyst **TPA-Zn** under full range light (black) and simulated visible light (red) irradiation. (c) A plot of hydrogen production every hour under full range (black) and visible light (red) irradiation. (d) Electrochemical impedence (Nyquist plot) of **TPA-Zn** under dark (black) and visible light exposure (red). (e) Mott–Schottky (MS) analysis for flat band potential of **TPA-Zn**. (f) Schematic representation of band positioning of **TPA-Zn** demonstrating thermodynamic feasibility towards photocatalytic H_2 evolution.

View Article Online
DOI: 10.1039/D0TA02318C

remains similar before and after photocatalysis (Figure S11). FESEM images also indicated retention of fibrous morphology after the photocatalysis (Figure S9). PXRD of **TPA-Zn** after the photocatalysis does not reveal additional sharp signals, discarding any possibility of hydrolysis of metal complex (Figure S7). After a photocatalytic experiment, **TPA-Zn** was removed by centrifugation and ICP-MS analysis of the resultant solution revealed the absence of zinc. All these experiments suggested a very good stability of **TPA-Zn** under the reaction condition. Such aqueous stability possibly resulted due to cooperatively enhanced Zn(II)-terpyridine binding constant in the polymer backbone.

To gain more insight of the photocatalysis process, light response on charge mobility of **TPA-Zn** was experimented by electrochemical impedance measurement under dark and visible light illumination (Figure 4d). The measurement was carried out utilizing aqueous 0.5 M Na_2SO_4 solution as the electrolyte, under an applied bias of –1.5 V vs. Ag/AgCl. The experiment displayed a much smaller semicircle under visible light than that of dark condition, signifying decrease in charge transfer resistance at the **TPA-Zn**/electrolyte interface upon light illumination. The lesser resistance is indicative for an easier promotion of electron to the conduction band which transfers electron to the proton (Figure 4f). Furthermore, the flat-band potential of **TPA-Zn** at pH = 7.8 (aqueous 0.5 M Na_2SO_4 electrolyte) was determined by electrochemical impedance spectroscopy using the Mott–Schottky (MS) method (Figure 4e). The MS plot revealed n-type semi-conducting nature of **TPA-Zn** with the conduction band edge potential of -0.50 V (vs NHE). The potential is more negative than that of water splitting (-0.46 V vs NHE), providing experimental support for successful photocatalytic activity of **TPA-Zn** (Figure 4f). As the DFT analysis showed the presence of HOMO over TPA unit, we assume that the TPA unit in **TPA-Zn** acts as catalytic centre (proton binding site), whereas Zn^{II} remains inactive due to its d^{10} electronic configuration. Notably, utilization of Fe(II), Co(II) and Ni(II) resulted photocatalytic dihydrogen production in the micromolar/gram scale (Figure S13).

In summary, we have presented a novel coordination polymer **TPA-Zn** having significantly high photocatalytic activity for hydrogen generation with 2.9% quantum efficiency at 400 nm. The design principle of the water-splitting photocatalyst relies on intermittent disruption of conjugation by Zn^{II} metal nodes to provide a suitable amount of exciton separation ability and charge carrier mobility. The Mott-schotky analysis confirmed the feasibility of successful electron transfer from **TPA-Zn** to proton during photocatalytic H_2 evolution. Notably, the millimole per gram scale hydrogen production was achieved without co-catalyst. The observation paves a new way to realize TPA based moderately conjugated metal-organic hybrid material as an efficient hydrogen evolution photocatalyst.

D.S. thanks the Department of Science and Technology (DST), Government of India for funding of this work under the INSPIRE faculty award IFA-18/CH-312.

Conflicts of interest

There are no conflicts to declare.

Notes and references

1 A. Goeppert, M. Czaun, J.-P. Jones, G. K. S. Prakash and G. A. Olah, *Chem. Soc. Rev.* 2014, **43**, 7995–8048.

2 (a) D. J. Martin, G. Liu, S. J. A. Moniz, Y. Bi, A. M. Beale, J. Ye and J. Tang, *Chem. Soc. Rev.* 2015, **44**, 7808–7828; (b) V. W.-H. Lau, M. B. Mesch, V. Duppel, V. Blum, J. Senker and B. V. Lotsch, *J. Am. Chem. Soc.* 2015, **137**, 1064–1072; (c) V. R. Bakuru, M. E. Dmello and S. B. Kalidindi, *ChemPhysChem*, 2019, **20**, 1177-1215.

3 (a) R. Asahi, T. Morikawa, T. Ohwaki, K. Aoki and Y. Taga, *Science*, 2001, **293**, 269–271; (b) S. J. Davis, K. Caldeira and H. D. Matthews, *Science*, 2010, **329**, 1330–1333; (c) J. Ran, J. Zhang, J. Yu, M. Jaroniec and S. Z. Qiao, *Chem. Soc. Rev.* 2014, **43**, 7787–7812; (d) J. Qi, K. Zhao, G. Li, Y. Gao, H. Zhao, R. Yu and Z. Tang, *Nanoscale*, 2014, **6**, 4072–4077; (e) K. Zhao, S. Zhao, J. Qi, H. Yin, C. Gao, A. M. Khattak, Y. Wu, A. Iqbal, L. Wu, Y. Gao, R. Yu and Z. Tang, *Inorg. Chem. Front.* 2016, **3**, 488–493; (f) J. -Q. Jiang, X. -L. Chen, J. Lu, Y. -F. Li, T. Wen and L. Zhang, *Chem. Commun.*, 2019, **55**, 6499 - 6502.

4 (a) B. Zhu, R. Zou and Q. Xu, *Adv. Energy Mater.* 2018, **8**, 1801193; (b) Z. Wang, J. Huang, J. Mao, Q. Guo, Z. Chen and Y. Lai, *J. Mater. Chem. A*, DOI: 10.1039/c9ta12776c; (c) X. -Y. Dong, M. Zhang, R. -B. Pei, Q. Wang, D. -H. Wei, S. -Q. Zang, Y. -T. Fan and C. W. Mak, *Angew. Chem. Int. Ed.* 2016, **55**, 2073-2077.

5 (a) D. Dong, C. Yan, J. Huang, N. Lu, P. Wu, J. Wang and Z. Zhang, *J. Mater. Chem. A*, 2019, **7**, 24180–24185; (b) H. Wang and Z. Jin, *Sustainable Energy Fuels*, 2019, **3**, 173–183; (c) T. Liao, L. Kou, A. Du, Y. Gu and Z. Sun, *J. Am. Chem. Soc.* 2018, **140**, 9159 – 9166; (d) D. Samanta, P. Verma, S. Roy and T. K. Maji, *ACS Appl. Mater. Interfaces*, 2018, **10**, 23140–23146; (e) T. Wang, R. Jin, X. Wu, J. Zheng, X. Li and K. Ostrikov, *J. Mater. Chem. A,* 2018, **6**, 9228–9235; (f) H. Chen, Z. -G. Gu, S. Mirza, S. -H. Zhang and J. Zhang, *J. Mater. Chem. A*, 2018, **6**, 7175–7181.

6 (a) J. Liu, Y. Liu, N. Liu, Y. Han, X. Zhang, H. Huang, Y. Lifshitz, S.-T. Lee, J. Zhong and Z. Kang, Science 2015, **347**, 970–974; (b) F. Haase, T. Banerjee, G. Savasci, C. Ochsenfeld and B. V. Lotsch, *Faraday Discuss.* 2017, **201**, 247–276; (c) V. S. Vyas, F. Haase, L. Stegbauer, G. Savasci, F. Podjaski, C. Ochsenfeld and B. V. Lotsch, *Nat. Commun.* 2015, **6**, 8508; (d) T. Banerjee, F. Haase, G. Savasci, K. Gottschling, C. Ochsenfeld and B. V. Lotsch, *J. Am. Chem. Soc.* 2017, **139**, 16228–16234; (e) J. Wang, G. Ouyang, Y. Wang, X. Qiao, W. -S. Li and H. Li, *Chem. Commun.* 2020, **56**, 1601 – 1604.

7 (a) H. Hennig, *Angew. Chem., Int. Ed.* 2015, **54**, 4429; (b) J. Guo, Y. Zhang, L. Shi, Y. Zhu, M. F. Mideksa, K. Hou, W. Zhao, D. Wang, M. Zhao, X. Zhang, J. Lv, J. Zhang, X. Wang and Z. Tang, *J. Am. Chem. Soc.* 2017, **139**, 17964–17972; (c) Q. Lei, X. Long, H. Chen, J. Tan, X. Wang and R. Chen, *Chem. Commun.*, 2019, 55, 14478 - 14481.

8 C. Xu, W. Zhang, J. Tang, C. Pan and G. Yu, *Front. Chem.*, 2018, **6**, 592.

9 (a) V. S. Mothika, P. Sutar, P. Verma, S. Das, S. K. Pati and T. K. Maji, Chem. Eur. J. 2019, 25, 3867 – 3874; (b) G. Damas, C. F. N. Marchiori and C. M. Araujo, *J. Phys. Chem. C,* 2018, **122**, 47, 26876 - 26888; (c) J. Kosco, M. Bidwell, H. Cha, *et al. Nat. Mater.* (2020). DOI: 10.1038/s41563-019-0591-1

10 (a) X. Liu, L. He, J. Zheng, J. Guo, F. Bi, X. Ma, K. Zhao, Y. Liu, R. Song and Z. Tang, *Adv. Mater.* 2015, **27**, 3273 - 3277; (b) Y. Li, J. Tang, L. He, Y. Liu, Y. Liu, C. Chen and Z. Tang, *Adv. Mater.* 2015, **27**, 4075 - 4080; (c) S. Furukawa, J. Reboul, S. Diring, K. Sumida and S. Kitagawa, *Chem. Soc. Rev.* 2014, **43**, 5700–5734; (d) M. Zhao, K. Deng, L. He, Y. Liu, G. Li, H. Zhao and Z. Tang, *J. Am. Chem. Soc.* 2014, **136**, 1738 - 1741.

11 S. Roy, A. Bandyopadhyay, M. Das, P. P. Ray, S. K. Pati and T. K. Maji, *J. Mater. Chem. A*, 2018, **6**, 5587-5591.

12 D. Samanta, S. Roy, R. Sasmal, N. D. Saha, K. R. Pradeep, R. Viswanatha, S. S. Agasti and T. K. Maji, *Angew. Chem., Int. Ed.*, 2019, **58**, 5008–5012.